In Operando GISAXS Studies of Mound Coarsening in Electrochemical Homoepitaxy

Martin Ruge,[1] Frederik Golks,[1,2,*] Jörg Zegenhagen,[2] Olaf M. Magnussen,[1,†] and Jochim Stettner[1]
[1]*Institut für Experimentelle und Angewandte Physik, Christian-Albrechts-Universität Kiel, Leibnizstraße 19, D-24098 Kiel, Germany*
[2]*European Synchrotron Radiation Facility, 6 rue Jules Horowitz, BP 220, F-38043 Grenoble Cedex, France*
(Received 23 November 2013; published 6 February 2014)

Kinetic roughening during electrodeposition was studied by grazing incidence small angle x-ray scattering for the case of Au(001) homoepitaxial growth in Cl^- containing electrolytes. The formation and coarsening of an isotropic mound distribution on unreconstructed Au(001) and of [110]-oriented anisotropic mounds on the "hex" reconstructed surface was observed. The lateral mound coarsening is described by a well-defined scaling law. On unreconstructed Au a transition in the coarsening exponent from $\approx 1/4$ to $\approx 1/3$ with increasing potential is found, which can be explained by the pronounced potential dependence of surface transport processes in an electrochemical environment.

DOI: 10.1103/PhysRevLett.112.055503 PACS numbers: 61.05.cf, 68.08.-p, 68.35.Ct, 81.15.Pq

The evolution of the deposit morphology during electrochemical growth is a subject of great fundamental interest as well as of central importance for many applications, ranging from plating processes in the microelectronics industry to electrode reactions in batteries. Quantitative studies of the structural evolution of electrodeposits are still scarce, in particular, on the meso- and nanoscale. Even for the most simple case, homoepitaxial growth, it is still largely unclear how the electrochemical environment influences key properties, such as roughness and grain size.

In contrast, kinetic roughening during homoepitaxial deposition under vacuum conditions nowadays is much better understood. Numerous experimental and theoretical studies have revealed a variety of different scenarios, depending on film thickness and deposition parameters (see [1] and references therein). In particular, mound formation and coarsening in the multilayer growth regime as a result of unstable crystal growth has attracted considerable interest [2,3]. This growth behavior originates in an effective uphill current, caused by the presence of an Ehrlich-Schwoebel barrier that hinders adatom diffusion over descending steps. The resulting temporal evolution of the average lateral mound size obeys a power law $\xi(t) = \xi_0 t^n$. In some cases the slopes of the mounds approach a constant value ("slope selection"), i.e., the mounds have defined facets, while in others the slope increases.

Prototypical examples of perpetual mound coarsening are homoepitaxial growth processes on metal surfaces with square symmetry, such as Cu(001) [4,5] and Ag(001) [6,7]. For these systems coarsening exponents $n \approx 1/4$ or smaller were reported in the experimental studies. Various explanations for these exponents were proposed in simulations and theoretical studies, which typically found values between $1/4$ and $1/3$ for square symmetry substrates, depending on the system parameters [8–10]. Numerical studies either suggested that n crucially depends on the appearance of specific topological defects ("roof tops") [8] or attributed the different n values to the presence of rapid corner diffusion [9]. In contrast, a recent analytical analysis concluded that $n = 1/3$ for slope selection whereas otherwise $n = 1/4$ [10].

Up to now, kinetic roughening in an electrochemical environment was addressed only in *ex situ* microscopy growth studies of thick polycrystalline deposits [11,12]. Qualitatively, the initial stages of homoepitaxial electrodeposition on Au(001) [13] and Cu(001) [14] in chloride-containing electrolytes were investigated by *in situ* surface x-ray diffraction (SXRD), revealing a pronounced influence of the electrode potential and coadsorbed anions on the growth behavior. Specifically, for the Au(001) system studied here, growth in the regime where the Au surface is unreconstructed changes with decreasing deposition potential from step flow to first layer-by-layer (2D) and then to 3D growth. At even more negative potentials, where the phase transition to the "hex" reconstructed Au(001) surface occurs, a "reentrant" 2D growth is found. This potential-dependent growth behavior can be rationalized by electrostatic contributions to the activation energies of the underlying surface transport processes, caused by interactions of the strong interfacial field with the dipole moments of surface atoms [15].

As shown below, the surface morphology of metal electrodes under homoepitaxial deposition conditions is highly dynamic. Consequently, kinetic roughening in the initial stages of electrodeposition has to be studied *in operando* with a time resolution on the order of seconds. This severely hampers investigations by scanning tunneling (STM) and atomic force (AFM) microscopy. We therefore employ in this study grazing incidence small angle x-ray scattering (GISAXS), which is a powerful tool for elucidating the nanoscale surface structure under vacuum conditions [16]. GISAXS studies of kinetic roughening in gas phase homoepitaxial growth have up to now been limited to

a few selected systems [7,17–19]. The presence of isotropically distributed mounds manifests in these experiments as characteristic ring-shaped diffuse scattering. We here present time-dependent *in operando* GISAXS measurements for Au(001) electrodeposition in the potential regime of 3D growth, where the lateral mound coarsening was determined from this diffuse scattering.

The experiments were performed at the ID32 beam line of the European Synchrotron Radiation Facility using a photon energy of 22.5 keV and a beam size of $250 \times 25\ \mu m^2$. As in the previous SXRD studies [13,14] we employed a "hanging meniscus" x-ray transmission cell with an Ag/AgCl (3M KCl) reference electrode. As a working electrode we used hat-shaped, polished Au(001) single crystals (MaTecK, 99.999%, diameter 4 mm, miscut $< 0.1°$, mosaic spread $< 0.2°$). The crystals were flame annealed in a butane gas flame prior to the experiments. As electrolyte 0.1 M $HCl + x$ mM $HAuCl_4$ ($x = 0.5,\ 1$), prepared from suprapure HCl (Merck), $HAuCl_4$ (Chempur), and Milli-Q water (18.2 MΩ cm) was employed, corresponding to diffusion-limited deposition rates of 4 ML min^{-1} and 8 ML min^{-1}, respectively [13]. Oxygen was removed from the electrolyte and x-ray cell by flushing with argon (6.0). The GISAXS data were recorded with a two-dimensional detector (Dectris Pilatus 300K–W), placed 1.5 m behind the sample and perpendicular to the primary beam (Fig. 1). In front of the detector a tantalum strip ($29 \times 2\ mm^2$) was mounted as a beam stop for the primary and reflected beam. The incident beam angle α_i was kept at 0.2°, which is close to the critical angle.

In the experiments, the following procedure was employed: The potential was stepped at $t = 0$ s from 0.6 V, i.e., the potential regime of step flow growth, to a more negative potential E_{end} in the 3D growth regime (−0.1 to 0.2 V), while the two-dimensional detector recorded the scattered intensity with an image acquisition rate of 0.5 Hz. At $t = 100$ s the potential was switched back to 0.6 V, resulting in a recovery of the initial smooth surface within seconds. Detector frames taken during step flow growth prior to the potential steps only exhibit scattering at low in-plane scattering vectors ($q_\parallel \leq 0.01\ Å^{-1}$). Those result from residual contributions of the specularly reflected and primary beam as well as scattering contributions from the μm scale step arrangement caused by the sample miscut. In contrast, detector frames taken during 3D growth exhibit additional diffuse scattering at larger in-plane vectors $q_\parallel$, resulting from the growing, rough surface. For an easier analysis and visualization of the scattering by the mounds, the (time-independent) low-q intensity was removed by subtracting the intensity distribution averaged over frames recorded at $t < 0$ from the data (see Supplemental Material [20]).

Examples of the resulting intensity maps at various times t of a growth experiment on the unreconstructed Au(001) surface, plotted as a function of the in-plane components q_x and q_y of the scattering vector, are shown in Fig. 2(a) and reveal pronounced intensity changes during the deposition process (a video showing all frames of this experiment is provided in the Supplemental Material [20]). At deposition times $t \geq 4$ s the diffusely scattered intensity is concentrated on a continuous ring ("Henzler ring") with a time-dependent radius q_r indicating formation and coarsening of isotropic mounds with characteristic lateral sizes $\xi = 2\pi/q_r$. As clearly visible in the corresponding radial intensity distribution $I(q_\parallel)$ [Fig. 2(b)], the ring diameter decreases and its intensity increases significantly with deposition time, indicating that the mounds grow in lateral size ξ as well as in height. A similar behavior was observed at other potentials ≥ -0.05 V, where the surface is unreconstructed.

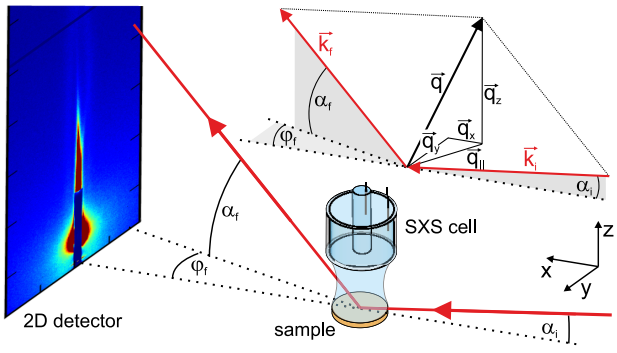

FIG. 1 (color online). Schematic illustration of the experimental and the scattering geometry of the *in situ* GISAXS measurements.

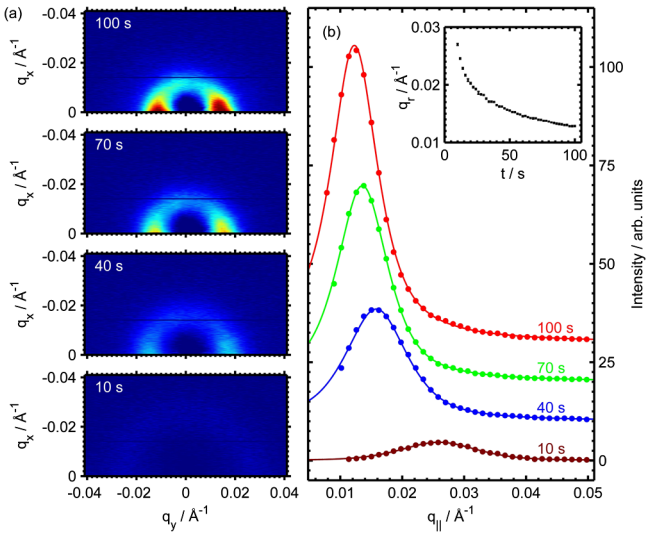

FIG. 2 (color online). (a) Intensity distribution $I(q_x, q_y)$ at different stages of 3D growth on the unreconstructed Au(001) surface at $E_{end} = 0.1$ V. (b) Corresponding radial intensity distribution $I(q_\parallel)$ (symbols) together with fits (lines) based on Lorentzian peak line shapes (error bars are smaller than the symbol size). For clarity the curves are vertically shifted with respect to each other. The inset shows the peak position q_r as a function of deposition time.

Quantitative data on the temporal evolution of the lateral mound size $\xi(t)$ indicate a well-defined coarsening process [Fig. 3(a)]. In particular, at all potentials and both deposition rates a defined power law is found for $t \geq 15$ s, demonstrating that the scaling hypothesis is also valid for mound coarsening during electrodeposition at the solid-liquid interface. Deviations are only observed in the initial stages of deposition at deposit coverages up to 1 ML, where nucleation and the formation of the initial mound distribution occur. Although $\xi(t)$ exhibits defined scaling under all experimental conditions, the growth behavior strongly depends on deposition parameters. Both the prefactor ξ_0 as well as the coarsening exponent n significantly increase with potential [Figs. 3(b),(c)], indicating larger lateral mound sizes and faster coarsening processes for more positive potentials. Because of this, the characteristic mound size after 100 s deposition more than doubles over the 300 mV wide potential window of 3D growth. In contrast, the deposition rate did not significantly influence the morphological evolution. However, the Au ion concentration and thus the (diffusion-limited) deposition rate of the employed electrolytes in the experiments only varied by a factor of 2 and, hence, may be negligible in comparison to the potential effects (see below).

The increase in mound size with increasing potential [Fig. 3(b)] can be easily rationalized by the well-known potential dependence of the Au surface mobility. Already, in early *in situ* STM studies of Au(001) in Au-free solutions, a significant increase of the decay of monolayer islands towards more positive potentials was reported, especially in Cl^- containing electrolytes [21]. Quantitative STM investigations of this process suggested an exponential increase of the island decay rate with potential and concluded that the sum of adatom formation energy and diffusion barrier decreased by 0.42 eV/V [15]. Because of this effect, the nucleation density in the initial stages of 3D island formation should decrease with potential. Furthermore, faster surface mass transport should qualitatively enhance the island coarsening and thus lead to larger coarsening exponents n, as indeed is observed in our experiments.

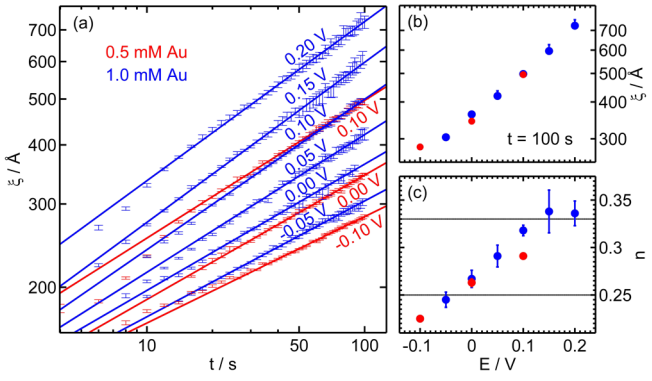

FIG. 3 (color online). (a) Lateral mound size ξ as a function of deposition time for various potentials in the 3D growth regime (symbols) together with best fits to a power law (lines). (b) Potential dependence of mound size ξ after $t = 100$ s and (c) coarsening exponent n.

A more detailed inspection of the potential-dependent coarsening behavior reveals a crossover from $n \approx 1/4$ for $E_{\text{end}} \leq -0.05$ V to $n \approx 1/3$ at $E_{\text{end}} \geq 0.15$ V [Fig. 3(c)]. According to previous numerical and analytic studies, these two exponents seem to describe limiting cases in mound coarsening of square systems [1–3,8–10]. For comparison of those studies with our results we have to consider that according to the STM observations [15,21] adatoms can easily detach from the island edges, corresponding to reversible island formation. In addition, previous qualitative SXRD studies of electrochemical Au(001) growth indicate the presence of a significant (potential-dependent) Ehrlich-Schwoebel barrier in the 3D growth regime [13]. Under these conditions Amar reported exponents $n \approx 1/4$ for a small ratio of terrace diffusion constant to flux (5×10^3) and $n \approx 1/3$ for a large ratio (10^5), which was rationalized by an effective corner diffusion in the second case [9]. This accurately describes the results obtained in the Au(001) electrodeposition system, where the Au surface diffusion strongly increases with potential (the flux is constant in our experiments). Siegert ascribed the coarsening of square pyramidal mounds to the elimination of roof-top-like defects and found an exponent of 1/4 [8]. However, n was 1/3 in the case that the coarsening was no longer enslaved to the dynamics of roof tops, which depends on microscopic processes, such as edge diffusion. These results were somewhat challenged by Biagi *et al.* who found the exponent to depend on the presence of slope selection [10]. Following the latter analysis, the change in n from 1/4 to 1/3 observed in our study would indicate a crossover from mounds without slope selection to mounds with faceted side walls, which should be testable in future studies.

Interestingly, experimental studies of gas phase homoepitaxial growth in very similar systems, e.g., Cu(001) and Ag(001), only found exponents n of (up to) $\approx 1/4$, but no crossover to $n = 1/3$ [1,4–7]. However, temperature and flux were fixed or varied over a rather limited range in these studies. In contrast, the variation of the growth conditions in the experiments described here is substantial. For Au(001) in Cl-containing electrolytes the relevant activation energies for surface transport should change by $\approx 15\%$ over the potential range employed in our study according to Ref. [15]. On the other hand, the effect of the potential on the surface dynamics fundamentally differs from temperature effects, which equally affect all elementary processes. Since the potential-dependent electrostatic energy contributions to the free energies are determined by the corresponding changes in the surface dipole moment, the dynamics of different surface processes can be influenced to a different extent. This may result in a selective enhancement of certain microscopic processes,

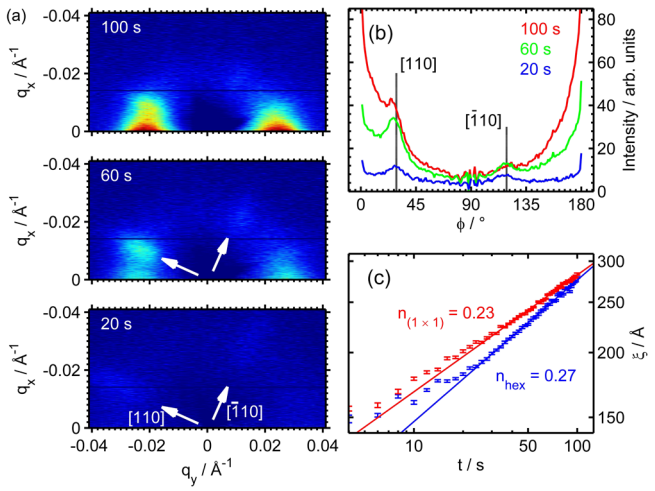

FIG. 4 (color online). (a) Intensity distribution $I(q_x, q_y)$ at different stages of 3D growth on the partially reconstructed Au(001) surface ($E_{\mathrm{end}} = -0.1$ V). In addition to the isotropic intensity distribution along the ring with radius q_r, peaks of enhanced intensity along the [110] and the $[\bar{1}10]$ direction are visible. (b) Corresponding azimuthal intensity distribution $I(\varphi)$ at $0.01\ \text{Å}^{-1} \leq q_{\parallel} \leq 0.04\ \text{Å}^{-1}$ and (c) $\xi(t)$ for the anisotropic (blue) and isotropic (red) surface structures.

which in turn can affect the evolution of the deposit morphology.

In addition, the electrochemical environment allows direct investigations of the influence of the hex Au(001) surface reconstruction on the kinetic roughening. At the onset of the potential-induced formation of the hex phase we observe in parallel to the isotropic scattering contributions distinct peaks at defined $q_{\parallel}$, which are rotated by an angle $\Delta\varphi = 90°$ with respect to each other around the origin of the q_x-q_y plane [Figs. 4(a),(b)]. In-plane rotation of the sample results in a corresponding rotation of these peaks, verifying that they are caused by an anisotropy of the deposit, leading to preferred characteristic length scales along the [110] and $[\bar{1}10]$ directions. These results are in good agreement with *in situ* STM studies of homoepitaxial electrodeposition on Au(001) [22]. Although these were obtained at much lower deposition rates (0.05 ML/ min) and in the layer-by-layer growth regime, the STM study also found anisotropic growth with the (reconstructed) monolayer islands oriented parallel to the hex stripes on the reconstructed surface, whereas on the unreconstructed surface isotropic islands were formed [22]. On the basis of the STM observations we attribute the intensity peaks in the GISAXS data to the shorter range correlations between parallel running anisotropic islands in the direction perpendicular to the islands orientation. The length scale along the island direction is much larger, i.e., it will be superimposed by the strong background scattering at low $q_{\parallel}$ and, hence, is not accessible.

The mound coarsening on the hex reconstructed surface was determined from the radial position of the intensity peaks and compared to that of the isotropic mounds on unreconstructed surface areas, which was determined from the parallel observed, ring-shaped diffuse scattering [Fig. 4(c)]. Interestingly, $\xi(t)$ on the hex surface initially is smaller than that of the unreconstructed mounds formed at the same potential, but coarsens considerably faster in the coverage regime > 1 ML. This increase in the exponent can be attributed to the enhanced Au surface mobility on the hex reconstruction, which also manifests in the crossover to reentrant layer-by-layer growth at even more negative potentials [13].

In summary, our *in operando* GISAXS study of Au(001) electrodeposition reveals kinetic roughening with a well-defined, potential-dependent scaling of the mound coarsening. This is not only of practical importance for a better understanding of deposit morphology evolution, which is of considerable technological relevance, but also of interest for basic growth physics: The possibility to tune the potential energy surface (and thus the rates of elementary transport processes) and even the surface structure (i.e., reconstruction) by the applied electrode potential is attractive for fundamental studies of kinetic roughening. As discussed above, changes of the activation energies by a few hundred meV are easily achievable, providing access to a large range of the relevant deposition parameters and thus new tests of theories and simulations in this extensive field.

We thank the European Synchrotron Radiation Facility for providing beam time, the ID32 staff for technical assistance, and the Deutsche Forschungsgemeinschaft for financial support via MA 1618/13.

*Present address: Robert Bosch GmbH, Postfach 10 60 50, 70049 Stuttgart, Germany.
†magnussen@physik.uni-kiel.de

[1] J. W. Evans, P. A. Thiel, and M. C. Bartelt, Surf. Sci. Rep. **61**, 1 (2006).
[2] P. Politi, G. Grenet, A. Marty, A. Ponchet, and J. Villain, Phys. Rep. **324**, 271 (2000).
[3] C. Misbah, O. Pierre-Louis, and Y. Saito, Rev. Mod. Phys. **82**, 981 (2010).
[4] J.-K. Zuo and J. F. Wendelken, Phys. Rev. Lett. **78**, 2791 (1997).
[5] F. Rabbering, H. Wormeester, F. Everts, and B. Poelsema, Phys. Rev. B **79**, 075402 (2009).
[6] W. C. Elliott, P. F. Miceli, T. Tse, and P. W. Stephens, Phys. Rev. B **54**, 17938 (1996).
[7] J. Alvarez, E. Lundgren, X. Torrelles, and S. Ferrer, Phys. Rev. B **57**, 6325 (1998).
[8] M. Siegert, Phys. Rev. Lett. **81**, 5481 (1998).
[9] J. G. Amar, Phys. Rev. B **60**, R11317 (1999).
[10] S. Biagi, C. Misbah, and P. Politi, Phys. Rev. Lett. **109**, 096101 (2012).
[11] S. Huo and W. Schwarzacher, Phys. Rev. Lett. **86**, 256 (2001).
[12] A. Osafo-Acquaah, Y. Shapir, and J. Jorne, J. Electrochem. Soc. **153**, C535 (2006).

[13] K. Krug, J. Stettner, and O. M. Magnussen, Phys. Rev. Lett. **96**, 246101 (2006).
[14] F. Golks, J. Stettner, Y. Gründer, K. Krug, J. Zegenhagen, and O. M. Magnussen, Phys. Rev. Lett. **108**, 256101 (2012).
[15] E. Pichardo-Pedrero, G. L. Beltramo, and M. Giesen, Appl. Phys. A **87**, 461 (2007).
[16] G. Renaud, R. Lazzari, and F. Leroy, Surf. Sci. Rep. **64**, 255 (2009).
[17] D. W. Kisker, G. B. Stephenson, P. H. Fuoss, and S. Brennan, J. Cryst. Growth **146**, 104 (1995).
[18] A. Fleet, D. Dale, A. R. Woll, Y. Suzuki, and J. D. Brock, Phys. Rev. Lett. **96**, 055508 (2006).
[19] J. D. Ferguson, G. Arikan, D. S. Dale, A. R. Woll, and J. D. Brock, Phys. Rev. Lett. **103**, 256103 (2009).
[20] See Supplemental Material at http://link.aps.org/supplemental/10.1103/PhysRevLett.112.055503 for a detailed description of data analysis and a video, which shows a full series of intensity maps taken during a potential step experiment.
[21] J. R. Nichols, O. M. Magnussen, J. Hotlos, T. Twomey, R. J. Behm, and D. M. Kolb, J. Electroanal. Chem. **290**, 21 (1990).
[22] C. Vaz-Domínguez and A. Cuesta, Electrochim. Acta **56**, 6847 (2011).